Neurobiology of Learning and Memory 135 (2016) 146–151

Contents lists available at ScienceDirect

Neurobiology of Learning and Memory

journal homepage: www.elsevier.com/locate/ynlme

In vivo two-photon imaging of striatal neuronal circuits in mice

Masaaki Sato [a,b,*,1], Masako Kawano [a], Yuchio Yanagawa [c], Yasunori Hayashi [a,d,e,f]

[a] *RIKEN Brain Science Institute, Wako, Saitama, Japan*
[b] *PRESTO, Japan Science and Technology Agency, Kawaguchi, Saitama, Japan*
[c] *Department of Genetic and Behavioral Neuroscience, Gunma University Graduate School of Medicine, Maebashi, Gunma, Japan*
[d] *Brain Science Institute, Saitama University, Saitama, Japan*
[e] *School of Life Science, South China Normal University, Guangzhou, China*
[f] *Department of Pharmacology, Kyoto University Graduate School of Medicine, Kyoto, Japan*

ARTICLE INFO

Article history:
Received 2 May 2016
Revised 6 July 2016
Accepted 7 July 2016
Available online 8 July 2016

Keywords:
Two-photon microscopy
Striatum
Basal ganglia
Deep brain imaging
Adeno-associated virus
In utero electroporation

ABSTRACT

Imaging studies of the subcortical striatum *in vivo* have been technically challenging despite its functional importance in movement control and procedural learning. Here, we report a method for imaging striatal neuronal circuits in mice *in vivo* using two-photon microscopy. Cell bodies and intermingled dendrites of GABAergic neurons labeled with fluorescent proteins were imaged in the dorsal striatum through an imaging window implanted in the overlying cortex. This technique could be highly useful for studying the structure and function of striatal networks at cellular and subcellular resolutions in normal mice, as well as in mouse models of neurological disorders.

1. Introduction

The striatum is a part of the subcortical basal ganglia that plays a pivotal role in motor control, motivation and procedural learning (Graybiel, 2005; Nelson & Kreitzer, 2014). Its dysfunction is known to cause neurological disorders, such as Huntington's disease and Parkinson's disease, which are characterized by difficulty in initiating and controlling movement. Research has revealed that the striatal circuits consist of a large number of anatomically intermingled, GABAergic spiny projection neurons and a smaller number of interneurons, such as large cholinergic interneurons, arranged between them (Kawaguchi, 1997). Moreover, the striatum is known to form two distinct parallel pathways: the dopamine D1 receptor-expressing direct pathway and the D2 receptor-expressing indirect pathway. The anatomical organization of the striatum is thus somewhat different from that of the cerebral cortex and hippocampus, where the basic feedforward circuits are constructed by glutamatergic excitatory neurons arranged into layers.

These striking features of striatal circuits have raised the possibility that a principle of neural circuit operation that is different from those of excitatory circuits may be visualized if we could study the structure and function of striatal neuronal circuits using *in vivo* imaging techniques. Despite the technical difficulty in gaining optical access to subcortical striatal neurons, a few studies so far have succeeded in optically recording striatal neural circuit activity by using microprobes or optical fibers (Bocarsly et al., 2015; Cui et al., 2013; Goto et al., 2015; Luo, Volkow, Heintz, Pan, & Du, 2011). To image the neuronal circuits under the neocortex at cellular and subcellular resolutions, two-photon imaging through an implanted window has been performed successfully for the hippocampus (Dombeck, Harvey, Tian, Looger, & Tank, 2010; Mizrahi, Crowley, Shtoyerman, & Katz, 2004; Sato et al., 2015). However, the applicability of this method for striatal imaging has not yet been explored. In this study, we established a procedure for high-resolution two-photon imaging of striatal neurons *in vivo* through an implanted imaging window.

Abbreviation: DTI, direct two-photon imaging through an implanted window.

* Corresponding author at: RIKEN Brain Science Institute, 2-1 Hirosawa, Wako, Saitama 351-0198, Japan.
E-mail addresses: msato@brain.riken.jp, masasato@mail.saitama-u.ac.jp (M. Sato).
[1] Present address: Brain Science Institute and Graduate School of Science and Engineering, Saitama University, 255 Shimo-okubo, Sakura-ku, Saitama, Saitama 338-8570, Japan.

http://dx.doi.org/10.1016/j.nlm.2016.07.006
1074-7427/

2. Materials and methods

2.1. Fluorescent labeling of striatal and cortical neurons

This study was performed in accordance with the institutional guidelines and protocols approved by the RIKEN Animal Experiments Committee.

An adeno-associated virus serotype 9 vector harboring a green fluorescent protein (GFP) gene downstream of the chicken beta-actin (CBA) promoter (AAV9-CBA-GFP, titer 1.08×10^{13} vg/ml, Virovek, Hayward, CA) was diluted 1:50–100 with phosphate-buffered saline (PBS) and was infused into the left dorsal striatum of C57BL/6J mice at 1–2 months of age using a glass pipette connected to a 10 μl syringe via polyethylene tubing at a rate of 0.3 μl/min (1.5–3 μl of total infusion volume). The coordinates were 0.4 mm posterior and 1.8 mm lateral to the bregma, where the primary somatosensory cortex overlies the dorsal striatum (Franklin & Paxinos, 2007), and 2.2 mm deep from the skull surface. After termination of infusion, the pipette was left undisturbed for an additional 2 min to avoid backflow. The glass pipette was then withdrawn from the brain, and the incised scalp was closed with surgical clips. After surgery, the mice were returned to their home cages and allowed to recover until imaging experiments or perfusion. Strong GFP expression in the dorsal striatum was typically observed from approximately 2 weeks after infusion.

Transfection of cortical neurons with plasmids expressing GFP-fused actin (GFP-actin) downstream of the CAG promoter by *in utero* electroporation was performed essentially as described (Tabata & Nakajima, 2001). Briefly, 1 μl of the plasmid DNA solution (dissolved at 2 μg/μl in 10 mM Tris-HCl, pH 8.0, and 1 mM EDTA containing 0.05% Fast Green) was pressure injected into lateral ventricles of C57BL/6J embryos on embryonic day 13.5. Four 33-V electrical pulses of 50 ms duration at 950 ms intervals were then delivered to the embryo heads using tweezer-type electrodes (CUY650P3, Nepa Gene Co. Ltd., Chiba, Japan) connected to a pulse generator (CUY21EDIT, BEX Co. Ltd., Tokyo, Japan).

2.2. Immunofluorescence microscopy

The mice were deeply anesthetized with Avertin and were perfused transcardially with PBS, followed by 4% paraformaldehyde (PFA) in PBS. Their brains were removed and further fixed in 4% PFA at 4 °C overnight. Coronal sections were cut using a microslicer to a thickness of 50 μm. The sections were incubated at 4 °C overnight with rabbit anti-Iba1 antibody (1:1000, 019-19741, Wako Pure Chemical Industries, Ltd., Osaka, Japan), rabbit anti-glial fibrillary acidic protein (GFAP) antibody (1:1000, N1506, Dako, Glostrup, Denmark), mouse anti-NeuN antibody (1:500–1:1000, MAB377, Millipore, Billerica, MA), rabbit anti-GABA antibody (1:1000, A2052, Sigma-Aldrich, St. Louis, MO) or goat anti-choline acetyltransferase (ChAT) antibody (1:5000, AB144P, Millipore) diluted in PBS containing 2% normal goat serum, 1% BSA and 0.1% Triton X-100, followed by Alexa Fluor 594-labeled goat anti-mouse, anti-rabbit IgG antibody (1:1000, A-11032 or A-11037, Thermo Fisher Scientific, Waltham, MA) or Cy3-labeled donkey anti-goat IgG antibody (1:1000, AP180C, Millipore) diluted in the same buffer at room temperature for 1 h. The GFP and Venus signals shown in all the images represent their native fluorescence. Fluorescence images were acquired using a Keyence BZ-9000 epi-fluorescence microscope equipped with a 4× objective (Keyence, Osaka, Japan) or an Olympus FV1000 laser-scanning confocal microscope equipped with a 60× water immersion objective (Olympus, Tokyo, Japan).

2.3. Direct two-photon imaging through an implanted window (DTI) for striatal neuronal circuits in vivo

The mice that received viral vector- or *in utero* electroporation-mediated gene transfer or transgenic mice expressing the yellow fluorescent protein Venus under the vesicular GABA transporter promoter (VGAT-Venus mice, Wang et al., 2009) were anesthetized with isoflurane (3% induction, 1.5% maintenance) supplemented with chlorprothixene (1 mg/kg, i.p.) and placed in a stereotaxic frame. Atropine (0.3 mg/kg, s.c.) and dexamethasone (2 mg/kg, s.c.) were administered prior to anesthesia to reduce respiratory secretions and brain edema, respectively. Surgery for implantation of an imaging window was performed as follows (Fig. S1). A circular piece of scalp was removed, and the underlying bone was cleaned and dried (Fig. S1A). A stainless steel head plate with a circular opening (7 mm diameter) was placed over the left parietal bone and attached to the skull with dental acrylic (Fig. S1B). A circular craniotomy was then made on the skull overlying the dorsal striatum. The dura was removed, and the overlying cortex was aspirated in small amounts using a blunted 25-gauge needle connected to a vacuum pump until the surface of the dorsal striatum was exposed (Fig. S1D). To reduce bleeding, aspiration started from a cortical area devoid of large vessels, and bleeding was treated promptly with a small piece of gelatin sponge (Spongel, Astellas Pharma, Tokyo, Japan) wetted with cortex buffer (123 mM NaCl, 5 mM KCl, 10 mM glucose, 2 mM $CaCl_2$, 2 mM $MgCl_2$, 10 mM HEPES, pH 7.4). *In vivo* labeling of astrocytes using the red fluorescent dye Sulforhodamine 101 (SR101) was performed by applying the dye solution (dissolved in cortex buffer at 100 μM) to the striatal surface for 5 min, followed by rinsing several times with cortex buffer. An imaging window, which consisted of a stainless steel ring (2.5 mm outer diameter, 2.2 mm inner diameter and 1.0 mm height) with a round coverslip (2.5 mm diameter, 0.17 mm thickness, Matsunami Glass Ind., Osaka, Japan) adhered to the bottom using UV-curable adhesive (NOA81, Norland Products, Cranbury, NJ), was then inserted to the cranial hole to support its surrounding tissue and the striatal surface mechanically. Once positioned, we ensured that the striatal surface was clearly observable through the bottom coverslip, devoid of any trace of bleeding (Fig. S1C and E). The upper rim was then affixed to the skull with dental acrylic.

The AAV infusion targeted to the dorsal striatal surface could inevitably result in GFP labeling of cells in the contiguous deep cortical layers in addition to the striatum (Fig. 1B). To avoid imaging residual cortical tissues, it is important to remove the cortex sufficiently until the underlying white matter is clearly exposed. The exposed white matter should then be gently peeled aside so that the underlying pinkish gray surface of the dorsal striatum is kept intact and visible (Fig. S1D).

After surgery, each mouse was placed under the microscope objective via the head plate. Body temperature was maintained at 37 °C with a heating pad throughout the imaging sessions. Images were acquired using a custom-built microscope equipped with a 25× NA1.05 objective (Olympus) or an Olympus FV1000MPE microscope equipped with a 40× NA0.8 objective (Olympus) in 512 × 512 or 1024 × 1024 pixels. Because the cortex overlying the dorsal striatum is more anterior and thicker than that overlying the dorsal hippocampus, the 40× objective with a longer working distance (3.3 mm) allowed more working space and imaging depth than the 25× objective that we previously used for hippocampal imaging (working distance 2.0 mm; Sato et al., 2015). GFP and Venus were excited using a Ti:sapphire laser (Tsunami or MaiTai DeepSee eHP, Spectra-Physics, Santa Clara, CA) at 910 nm, and the fluorescence was imaged using a 495–540-nm bandpass filter and a GaAsP photomultiplier tube. For dual color imaging, SR101 was simultaneously excited at 910 nm, and the sig-

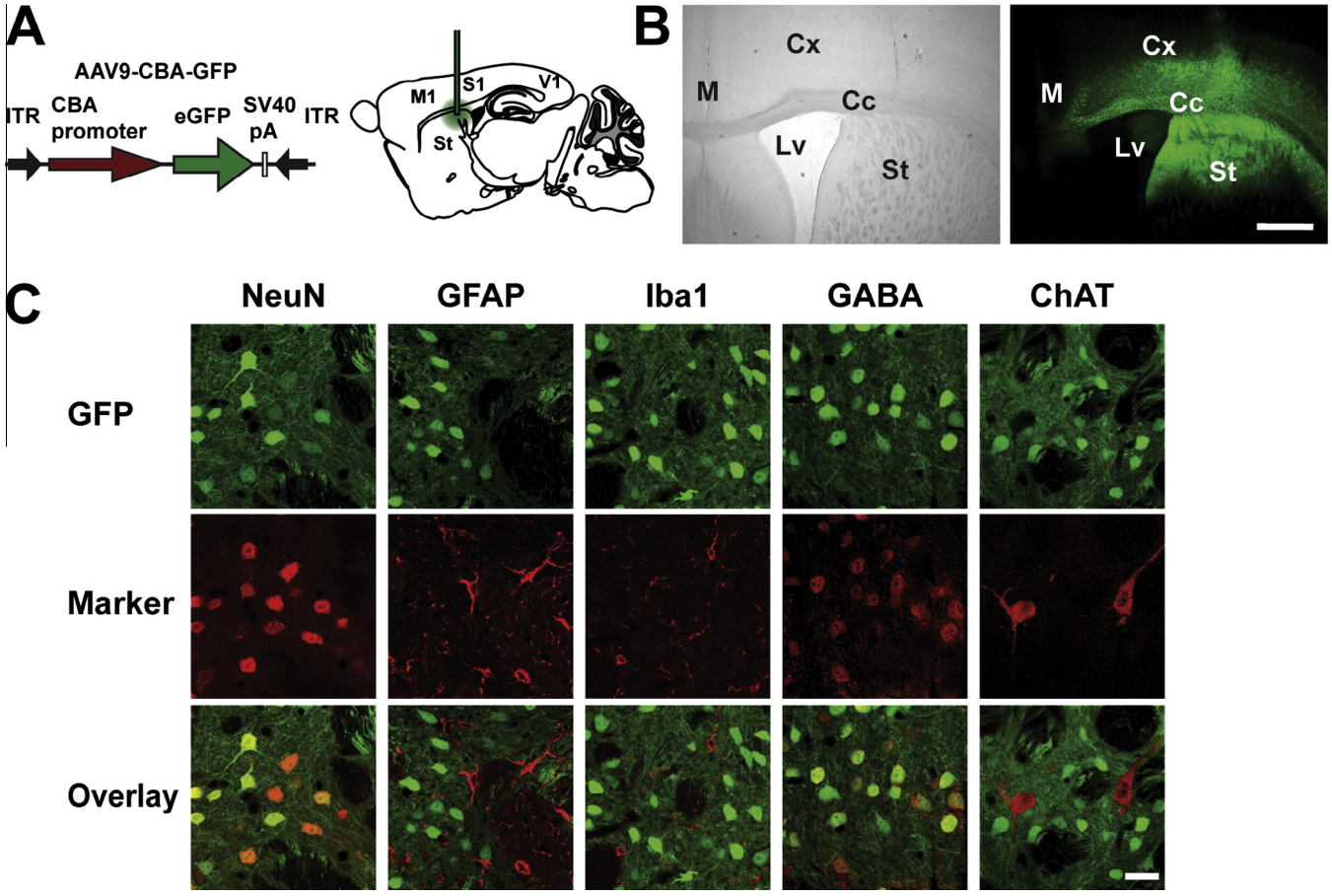

Fig. 1. GFP labeling of dorsal striatal neurons by AAV9-CBA-GFP. (A) Design of the AAV9-CBA-GFP vector (left) and microinfusion of the vector into the dorsal striatum (right). eGFP, enhanced green fluorescent protein; ITR, inverted terminal repeat; SV40pA, SV40-derived poly(A) signal; M1, primary motor cortex; S1, primary somatosensory cortex; St, striatum; V1, primary visual cortex. (B) Phase contrast (left) and GFP fluorescence images (right) obtained from a coronal section of a mouse brain infused with AAV9-CBA-GFP vectors into the dorsal striatum. Cc, corpus callosum; Cx, cerebral cortex; Lv, lateral ventricles; M, midline. Scale bar = 500 μm. (C) Immunohistological characterization of GFP-labeled dorsal striatal cells 18–20 days after infusion of AAV9-CBA-GFP. Brain sections were immunolabeled using antibodies against the neuronal marker NeuN, the astroglial marker GFAP, the microglial marker Iba1, the GABAergic neuronal marker GABA or the marker for cholinergic interneurons choline acetyl transferase (ChAT). GFP fluorescence, immunofluorescence against the marker proteins (Marker) and the overlaid images are shown from top to bottom. Scale bar = 20 μm.

nal was separated by a 570 nm dichroic mirror and a 575–630-nm bandpass filter.

Footprints were obtained by painting the hind paws of mice with black ink and allowing them to walk spontaneously on a sheet of paper immediately before and one day after surgery.

3. Results and discussion

To visualize striatal circuits *in vivo*, we labeled neurons in the dorsal striatum by microinfusion of AAV9-CBA-GFP (Fig. 1A and B). Immunohistological characterization confirmed that the GFP-labeled cells were NeuN-positive neurons but not GFAP-positive astrocytes or Iba1-positive microglia (Fig. 1C). In addition, the cells labeled with GFP had medium-sized cell bodies and were primarily immunoreactive for the GABAergic neuronal marker GABA (Table 1) but not for the cholinergic interneuron marker ChAT (Fig. 1C), indicating that AAV9-CBA-GFP preferentially labeled GABAergic neuronal populations, most of which are known as spiny projection neurons, in the dorsal striatum.

The GFP-labeled striatal neurons were imaged by direct two-photon imaging through an implanted window (DTI) using an objective with a long working distance (Fig. 2A and B, see Section 2.3 for details). Scanning from the striatal surface into the dorsal striatum provided images of cell bodies and the intermingled dendrites of many GFP-labeled neurons at different focal depths

Table 1
Colocalization of GFP expression with GABA immunoreactivity 13–20 days after striatal infusion of AAV9-CBA-GFP.

GFP (+) GABA (+)/total GABA (+)	71.8 ± 19.5% (84/121 cells)
GFP (+) GABA (+)/total GFP (+)	89.7 ± 8.3% (84/95 cells)

Data represent mean ± SD (n = 4 fields from 2 mice, 2 fields per mouse, and 28–36 cells per field). The numbers in parentheses represent the sum of cell numbers counted.

(Fig. 2F–J and Movie S1). The images typically contained patchy regions of virtually no fluorescence, which corresponded to the white matter bundles that are anatomically characteristic of the striatum. The GFP-labeled cells imaged *in vivo* were negative for SR101 staining (Fig. 2C–E), which was consistent with the absence of GFP labeling in GFAP-positive astrocytes observed by immunofluorescence microscopy (Fig. 1C). In higher-magnification images, GFP-labeled protrusions indicative of dendritic spines were discernible on the dendrites of putative spiny projection neurons (Fig. 2K, see also Fig. S2). This finding demonstrated the superior resolution of two-photon imaging because such fine subcellular structures have not been previously visualized by other single-photon excitation-based imaging techniques in the striatum *in vivo* (Goto et al., 2015; Luo et al., 2011).

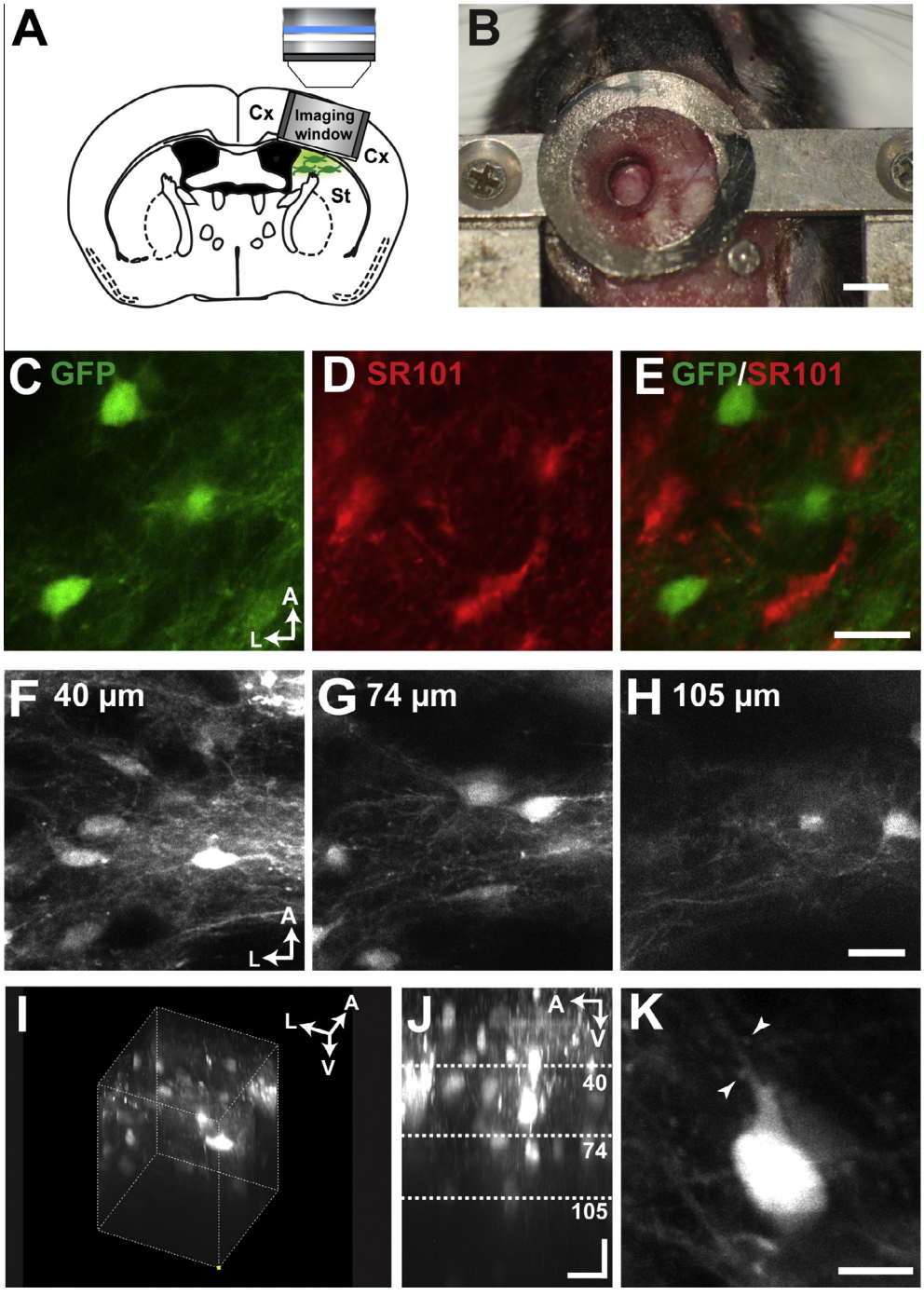

Fig. 2. Two-photon imaging of GFP-labeled striatal neurons *in vivo*. (A) Schematic representation of two-photon imaging of dorsal striatal neurons through an imaging window. (B) A photograph of an implanted imaging window for striatal imaging. Scale bar = 2 mm. (C–E) GFP-labeled cells (C) and SR101-labeled astrocytes (D) in the dorsal striatum imaged *in vivo* at a depth of 80 μm. The overlaid image is shown in (E). A, anterior; L, lateral. Scale bar = 20 μm. (F–H) A population of GFP-labeled dorsal striatal neurons imaged 40 (F), 74 (G) and 105 μm deep (H) from the striatal surface. Scale bar = 20 μm. (I and J) The image stack acquired from 0 to 150 μm from the striatal surface is shown as a three-dimensional reconstruction (I) and x-z projection (J). The depths at which the cells in (F)–(H) were imaged are indicated by dotted lines in (J). V, ventral. Scale bar = 20 μm. (K) Examples of GFP-labeled protrusions indicative of dendritic spines (arrowheads). Scale bar = 10 μm.

In addition to imaging virally labeled striatal GABAergic neurons, we imaged the dorsal striatum of VGAT-Venus transgenic mice with the same procedure (Fig. 3A). These mice were shown to have inhibitory neuronal populations of cells labeled with Venus in widespread brain areas (Wang et al., 2009). Implantation of the imaging window allowed us to visualize a population of Venus-labeled cells in the dorsal striatum of the transgenic mice (Fig. 3B and Movie S2). The appearance and distribution of the Venus-positive cells were consistent with those of Venus-labeled striatal neurons in the brain sections of the transgenic mice (Fig. 3C), confirming that DTI allowed reliable imaging of striatal GABAergic neuronal populations that were labeled virally or genetically with fluorescent proteins *in vivo*.

We further applied DTI for imaging of the subcellular components of striatal circuits *in vivo*. In the example shown in Fig. 3D and E, subcortically projecting neurons in the cingulate

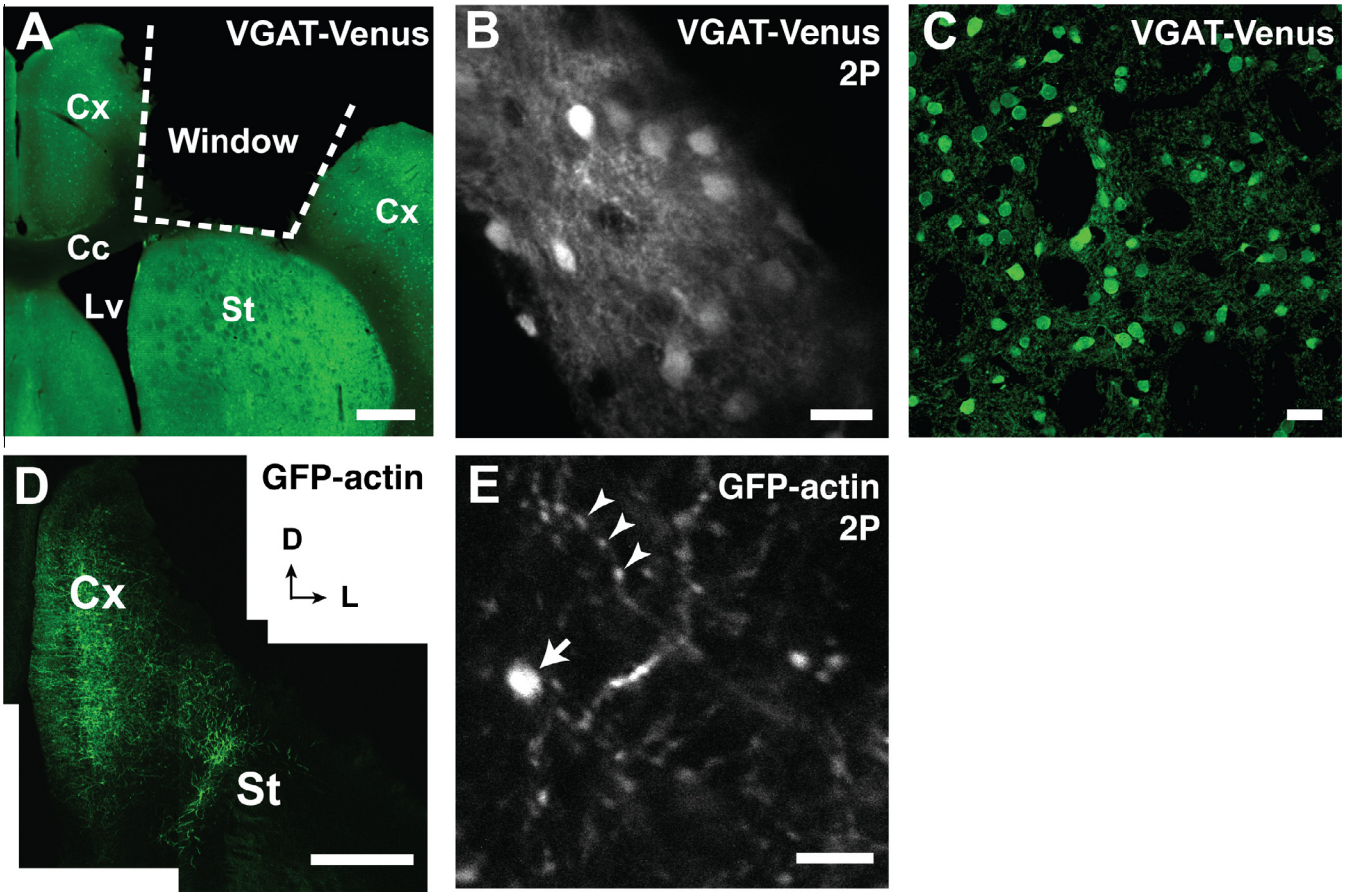

Fig. 3. *In vivo* two-photon imaging of dorsal striatal neurons labeled by Venus in VGAT-Venus transgenic mice and corticostriatal axons labeled by GFP-actin. (A) The imaging window (Window) was implanted over the dorsal striata of VGAT-Venus transgenic mice. Cx, cortex; Cc, corpus callosum; Lv, lateral ventricle; St, striatum. Scale bar = 500 μm. (B) Venus-labeled dorsal striatal neurons in VGAT-Venus transgenic mice imaged *in vivo* by two-photon microscopy (2P) through the implanted window. Scale bar = 20 μm. (C) Venus-labeled dorsal striatal neurons in VGAT-Venus transgenic mice imaged in a coronal section by confocal microscopy. Scale bar = 50 μm. (D) A montage of subcortically projecting neurons in the cingulate cortex transfected with GFP-actin by *in utero* electroporation. D, dorsal; L, lateral. Scale bar = 500 μm. (E) GFP-actin-labeled corticostriatal axons imaged *in vivo* by two-photon microscopy. Arrowheads indicate a few examples of GFP-actin-labeled varicosities. Arrow indicates a large varicosity. Scale bar = 10 μm.

cortex were transfected with GFP-actin by *in utero* electroporation, and the GFP-actin-labeled axons and associated varicosities were imaged in the dorsal striatum using DTI *in vivo* (Kincaid & Wilson, 1996; Zheng & Wilson, 2002) (Fig. 3D and E). This finding demonstrated the usefulness of DTI for imaging axonal fibers projecting to the striatum, as well as the cell bodies and dendrites of striatal neurons *in vivo*.

In this paper, we reported a procedure for high-resolution two-photon imaging of striatal neurons *in vivo* through an implanted imaging window. The procedure, termed DTI, can image different components of striatal neural circuits, including the soma and dendrites of spiny projection neurons and corticostriatal axons, at variable focal depths. In addition, it should be noted that the mice exhibited no apparent gait abnormalities after surgery, although the motor cortex was located near the site of window implantation (Fig. S3). This study opens the possibility for longitudinal imaging of striatal circuit activity during behavior in head-fixed configurations using genetically encoded calcium indicators (Bocarsly et al., 2015; Cui et al., 2013; Sato et al., 2015). This simple and reliable imaging procedure expands the applicability of imaging window implantation as a versatile technique for deep brain imaging, and it could be useful for imaging studies of striatal structures and function at cellular and subcellular resolutions in normal mice, as well as in mouse models of neurological disorders.

Acknowledgments

We thank Junichi Nakai for comments, Atsushi Miyawaki for the pCS2-Venus plasmid, and the staff of BSI-Olympus Collaboration Center for assisting with the imaging experiments. This work was supported by Strategic Programs for Research and Development (President's Discretionary Fund) at RIKEN and JSPS KAKENHI (16K13109) to M.S.

Appendix A. Supplementary material

Supplementary data associated with this article can be found, in the online version, at http://dx.doi.org/10.1016/j.nlm.2016.07.006.

References

Bocarsly, M. E., Jiang, W.-C., Wang, C., Dudman, J. T., Ji, N., & Aponte, Y. (2015). Minimally invasive microendoscopy system for in vivo functional imaging of deep nuclei in the mouse brain. *Biomedical Optics Express, 6*, 4546–4556.

Cui, G., Jun, S. B., Jin, X., Pham, M. D., Vogel, S. S., Lovinger, D. M., & Costa, R. M. (2013). Concurrent activation of striatal direct and indirect pathways during action initiation. *Nature, 494*, 238–242.

Dombeck, D. A., Harvey, C. D., Tian, L., Looger, L. L., & Tank, D. W. (2010). Functional imaging of hippocampal place cells at cellular resolution during virtual navigation. *Nature Neuroscience, 13*, 1433–1440.

Franklin, K. B. J., & Paxinos, G. (2007). *The mouse brain in stereotaxic coordinates* (3rd ed.) : . Academic Press.

Goto, A., Nakahara, I., Yamaguchi, T., Kamioka, Y., Sumiyama, K., Matsuda, M., ... Funabiki, K. (2015). Circuit-dependent striatal PKA and ERK signaling underlies rapid behavioral shift in mating reaction of male mice. *Proceedings of the National Academy of Sciences of the United States of America, 112*, 6718–6723.

Graybiel, A. M. (2005). The basal ganglia: Learning new tricks and loving it. *Current Opinion in Neurobiology, 15*, 638–644.

Kawaguchi, Y. (1997). Neostriatal cell subtypes and their functional roles. *Neuroscience Research, 27*, 1–8.

Kincaid, A. E., & Wilson, C. J. (1996). Corticostriatal innervation of the patch and matrix in the rat neostriatum. *Journal of Comparative Neurology, 374*, 578–592.

Luo, Z., Volkow, N. D., Heintz, N., Pan, Y., & Du, C. (2011). Acute cocaine induces fast activation of D1 receptor and progressive deactivation of D2 receptor striatal neurons: In vivo optical microprobe $[Ca^{2+}]_i$ imaging. *Journal of Neuroscience, 31*, 13180–13190.

Mizrahi, A., Crowley, J. C., Shtoyerman, E., & Katz, L. C. (2004). High-resolution in vivo imaging of hippocampal dendrites and spines. *Journal of Neuroscience, 24*, 3147–3151.

Nelson, A. B., & Kreitzer, A. C. (2014). Reassessing models of Basal Ganglia function and dysfunction. *Annual Review of Neuroscience, 37*, 117–135.

Sato, M., Kawano, M., Ohkura, M., Gengyo-Ando, K., Nakai, J., & Hayashi, Y. (2015). Generation and Imaging of transgenic mice that express G-CaMP7 under a tetracycline response element. *PLoS ONE, 10*, e015354.

Tabata, H., & Nakajima, K. (2001). Efficient in utero gene transfer system to the developing mouse brain using electroporation: Visualization of neuronal migration in the developing cortex. *Neuroscience, 103*, 865–872.

Wang, Y., Kakizaki, T., Sakagami, H., Saito, K., Ebihara, S., Kato, M., ... Yanagawa, Y. (2009). Fluorescent labeling of both GABAergic and glycinergic neurons in vesicular GABA transporter VGAT-venus transgenic mouse. *Neuroscience, 164*, 1031–1043.

Zheng, T., & Wilson, C. J. (2002). Corticostriatal combinatorics: The implications of corticostriatal axonal arborizations. *Journal of Neurophysiology, 87*, 1007–1017.